

Effect of interlayer exchange coupling in spin-torque nano oscillator

R. Arun^{1,1}, R. Gopal^{2,1}, V. K. Chandrasekar^{2,1, a)} and M. Lakshmanan¹¹

¹*Department of Nonlinear Dynamics, School of Physics, Bharathidasan University, Tiruchirappalli-620024, India*

²*Department of Physics, Centre for Nonlinear Science & Engineering, School of Electrical & Electronics Engineering, SASTRA Deemed University, Thanjavur- 613 401, India.*

(Dated: 16 August 2022)

The dynamics of the magnetization of the free layer in a spin-torque nano oscillator (STNO) influenced by a noncollinear alignment between the magnetizations of the free and pinned layers due to an interlayer exchange coupling has been investigated theoretically. The orientations of the magnetization of the free layer with that of the pinned layer have been computed through the macrospin model and they are found to match well with experimental results. The bilinear and biquadratic coupling strengths make the current to switch the magnetization between two states or oscillate steadily. The expressions for the critical currents between which oscillations are possible and the critical bilinear coupling strength below which oscillations are not possible are derived. The frequency of the oscillations is shown to be tuned and increased to or above 300 GHz by the current which is the largest to date among nanopillar-shaped STNOs.

I. INTRODUCTION

Since the discovery of the spin transfer torque (STT) effect by Slonczewski¹ and Berger², tremendous and continuous interest has been shown in the study of magnetization in STNOs because of its potential applications in magnetic memory technologies³⁻⁵. Compared to the conventional STT, creating and detecting spin polarized currents in the bilayer structures, consisting of heavy metal and ferromagnetic layers⁶⁻⁸, and trilayer structures where the ferromagnetic layers get separated by a non-magnetic layer, are important for the study of frequency enhancement^{9,10}, energy efficiency^{11,12}, fast magnetization switching¹² and spintronic-based neuromorphic computing systems¹³. In recent times, modern spintronic devices utilize multilayer structures where the coupling between the magnetic layers has to be controlled to get enhanced magnetic properties¹⁴. In an STNO the tunability in the thickness of the 3d, 4d and 5d nonmagnetic metallic spacer layer leads to ferromagnetic or antiferromagnetic coupling between the free and pinned ferromagnetic layers. This inter-layer exchange coupling has been intensively investigated since 1980s^{15-19,21}. Recent results in this context show that the presence of exchange coupling in a magnetic layer structure is mostly applicable to modern STT magnetic random-access memory (MRAM) and sensor devices¹⁷⁻¹⁹. In particular, the study of the interlayer exchange coupling effect in synthetic magnetic multilayer systems might provide a general strategy for beyond-CMOS electronic devices²⁰.

Very recently, Nunn *et al*²¹ have reported that a non-collinear alignment between the magnetizations of the free and pinned layers can be achieved and precisely controlled when they are coupled across a spacer layer consisting a non-magnetic material (Ru) alloyed with a ferromagnetic material (Fe). This noncollinear align-

ment happens due to the biquadratic coupling which can be tuned by changing the composition and thickness of the spacer layer²¹. This Co|RuFe|Co structure is useful for the noncollinear spintronic design with magnetic moments tilted to the film plane^{17-19,21}. Nevertheless, there is a lack of understanding about the impact of non-collinear alignment on the dynamics of the magnetization of the free layer in an STNO which is yet to be understood.

Therefore, in this paper, we theoretically investigate the influence of the noncollinear alignment due to the bilinear and biquadratic couplings in a Co|RuFe|Co STNO by numerically solving the underlying Landau-Lifshitz-Gilbert-Slonczewski (LLGS) equation. Our investigations confirm the existence of switching and high-frequency oscillations of the magnetization of the free layer due to current, in the presence of the bilinear and biquadratic exchange couplings. These studies open up new possibilities for the applications which utilize the current induced switching and high-frequency oscillations due to interlayer exchange coupling for the development of spintronic devices and neuromorphic computing devices^{23,24}. Sec. II addresses the governing equation, namely the Landau-Lifshitz-Gilbert-Slonczewski(LLGS) equation, for the magnetization dynamics of the free layer in Co|RuFe|Co STNO along with the bilinear and biquadratic exchange couplings. The current induced switching, oscillations of the magnetization of the free layer and its tunability by current and interlayer exchange coupling along with the expressions for the critical values of current and bilinear exchange coupling for the possibility of oscillations are presented in Sec. III. Finally, concluding remarks are made in Section IV. In Appendix A we have presented a methodology to identify the equilibrium orientation of the magnetization in the absence of the current using a microwave field. In Appendix B, the derivation for the critical values of the current and finally in Appendix C, we have discussed the output power and its enhancement.

^{a)}Electronic mail: chandru25nld@gmail.com

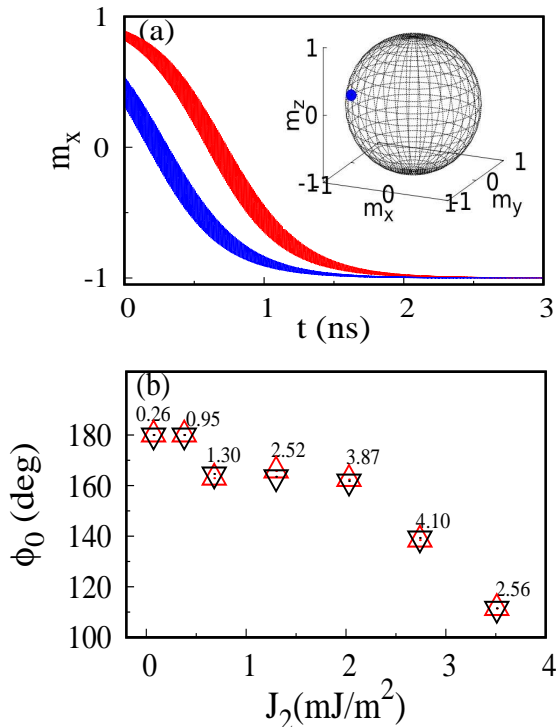


FIG. 1. (a) Time evolution of m_x for $I = 0$, $J_1 = 4.97$ mJ/m² and $J_2 = 0.919$ mJ/m². (b) The experimental (Red upward triangles) and the numerical values (black downward triangles) of $\phi_0 (= \cos^{-1}(m_{x0}))$ for different J_1 and J_2 corresponding to the spacer layer Ru₃₀Fe₇₀.

II. MODEL

We consider an STNO with a spacer layer Ru_{100-x}Fe_x consisting of a nonmagnetic material (Ru) alloyed with a ferromagnetic material (Fe)²¹. This layer is sandwiched between two ferromagnetic layers, which includes a free layer where the direction of the magnetization can change and a pinned layer where the magnetization is fixed along the positive x -direction. The plane of the layers is considered to be aligned with the xy -plane. The dynamics of the unit magnetization vector of the free layer \mathbf{m} is given by the LLGS equation

$$\frac{d\mathbf{m}}{dt} = -\gamma \mathbf{m} \times \mathbf{H}_{eff} + \alpha \mathbf{m} \times \frac{d\mathbf{m}}{dt} + \gamma H_S \mathbf{m} \times (\mathbf{m} \times \mathbf{p}), \quad (1)$$

In Eq.(1), $\mathbf{m} = m_x \mathbf{e}_x + m_y \mathbf{e}_y + m_z \mathbf{e}_z$ or $\mathbf{m} = (m_x, m_y, m_z)$, $|\mathbf{m}| = 1$. Here, $\mathbf{e}_x, \mathbf{e}_y$ and \mathbf{e}_z are the unit vectors along x, y and z directions, respectively. In spherical polar coordinates $m_x = \sin \theta \cos \phi$, $m_y = \sin \theta \sin \phi$ and $m_z = \cos \theta$, where θ and ϕ are polar and azimuthal angles, respectively. γ is the gyromagnetic ratio, α is the damping parameter and $H_S = H_{S0}/(1 + \lambda \mathbf{m} \cdot \mathbf{p})$,

where $H_{S0} = \hbar \eta I / 2eM_s V$ and $\mathbf{p} = \mathbf{e}_x$. Here I is the current passing through the free layer, $\hbar (= h/2\pi)$ is the reduced Planck's constant, e is the electron charge, M_s is the saturation magnetization and V is the volume of the free layer. The dimensionless parameters η and λ determine the magnitude and angular dependence of the spin-transfer torque. The energy density of the free layer is given by

$$E = \frac{J_1}{d} \mathbf{m} \cdot \mathbf{p} + \frac{J_2}{d} (\mathbf{m} \cdot \mathbf{p})^2 - \frac{M_s}{2} [H_k - 4\pi M_s] (\mathbf{m} \cdot \mathbf{e}_z)^2 \quad (2)$$

and the effective magnetic field $\mathbf{H}_{eff} = -\partial E / \partial (M_s \mathbf{m})$ of the free layer is

$$\mathbf{H}_{eff} = (H_k - 4\pi M_s) m_z \mathbf{e}_z - \frac{1}{dM_s} (J_1 + 2J_2 m_x) \mathbf{e}_x, \quad (3)$$

where J_1 and J_2 are the bilinear and biquadratic exchange coupling constants, respectively¹⁷. The effective field \mathbf{H}_{eff} includes the field due to bilinear and biquadratic couplings, magneto-crystalline anisotropy field H_k and demagnetization field $4\pi M_s$. In Eqs.(2) and (3), d is the thickness of the free layer. The material parameters are considered as $M_s = 1210$ emu/c.c., $H_k = 3471$ Oe, $\eta = 0.54$, $\lambda = \eta^2$, $d = 2$ nm, $A = \pi \times 60 \times 60$ nm², $V = Ad$, $\alpha = 0.005$ and $\gamma = 17.64$ Mrad/(Oe s)^{9-11,21,22}. Here A is the cross sectional area of the STNO. In this paper, J_1 is restricted to be positive, corresponding to the Fe concentration below 75% in the spacer, since oscillations are not observed for negative J_1 .

III. RESULTS AND DISCUSSION

Before applying any current the magnetization would settle in the xy -plane at $(m_{x0}, m_{y0}, m_{z0}) = (-1, 0, 0)$ when $J_1 \geq 2J_2$ or at $(-J_1/2J_2, \sqrt{1 - J_1^2/4J_2^2}, 0)$ when $J_1 < 2J_2$ ²¹. This is confirmed in Fig.1(a), where the time evolution of m_x is plotted for $J_1 = 4.97$ mJ/m² and $J_2 = 0.919$ mJ/m² for two different initial conditions and we can see that finally, \mathbf{m} reaches the state $(-1, 0, 0)$ (see the inset of Fig.1(a)) irrespective of the initial condition. Similarly, the polar angle $\phi_0 (= \cos^{-1}(m_{x0}))$ since $\theta_0 = \pi/2$, corresponding to (m_{x0}, m_{y0}, m_{z0}) is plotted for different sets of J_1 and J_2 in the absence of current and marked by downward black triangles in Fig.1(b). The values of ϕ_0 can also be determined using microwave field [see Appendix A]. The red upward triangles are the experimental values measured by Nunn *et al* corresponding to the spacer layer Ru₃₀Fe₇₀ which confirms the validation of the macrospin simulation²¹.

In the presence of current, the magnetization leaves the (m_{x0}, m_{y0}, m_{z0}) state and exhibits three kinds of dynamics depending upon the values of I and J_1 (or J_2). The magnetization \mathbf{m} may continue in the same initial state,

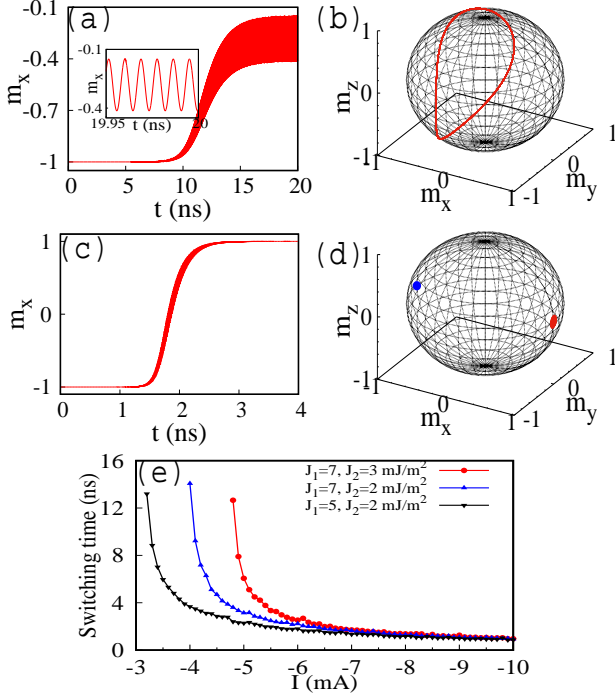


FIG. 2. Time evolution of m_x and trajectory of \mathbf{m} for (a-b) $I = -1.5$ mA and (c-d) $I = -5$ mA. Here, $J_1 = 4.97$ mJ/m² and $J_2 = 0.919$ mJ/m². (e) Variation of switching time versus current for different values of J_1 and J_2 . Inset in (a) corresponds to the oscillations for the time between 19.95 ns and 20 ns.

or switch from one to another state or oscillate. The magnetization \mathbf{m} switches to $(1, 0, 0)$ when $|I| > |I_c^{max}|$ or oscillates when $|I_c^{min}| < |I| < |I_c^{max}|$. When $|I| < |I_c^{min}|$ it continues to exist in $(-1, 0, 0)$ for $J_1 \geq 2J_2$ or switches to $(m_{x1}, m_{y1}, m_{z1}) \approx (m_{x0}, m_{y0}, m_{z0})$ for $J_1 < 2J_2$. Here I_c^{min} and I_c^{max} are the critical currents between which oscillations are possible, which can be derived as [see Appendix B for more details]

$$I_c^{max} = -\frac{\alpha e A (1 + \lambda)}{\hbar \eta} [2(J_1 + 2J_2) + (H_k - 4\pi M_s) d M_s], \quad (4)$$

$$I_c^{min} = \begin{cases} -\frac{\alpha e A (1 - \lambda)}{\hbar \eta} [2(J_1 - 2J_2) - (H_k - 4\pi M_s) d M_s] & \text{for } J_1 \geq 2J_2, \\ -\frac{\alpha e A (2J_2 - J_1 \lambda)^2}{\hbar \eta J_2} \left[\frac{2J_2 d M_s (H_k - 4\pi M_s) - (4J_2^2 - J_1^2)}{\lambda(4J_2^2 - J_1^2) - 2J_2(2J_2 - J_1 \lambda)} \right] & \text{for } J_1 < 2J_2. \end{cases} \quad (5)$$

In Figs.2(a-d), the time evolution and trajectories of \mathbf{m} corresponding to the oscillations and switching are plotted for $J_1 = 4.97$ mJ/m² and $J_2 = 0.919$ mJ/m². The values of I_c^{max} and I_c^{min} are calculated as -2.214 mA and

-1.026 mA from Eqs.(4) and (5), respectively. When the current is below -1.026 mA the magnetization continues to get settled at $(-1, 0, 0)$ as shown in the inset of Fig. 1(a). When $I = -1.5$ mA, the magnetization exhibits oscillations as shown in Figs. 2(a-b) and when $I = -5$ mA it switches from $m_x = -1$ to $+1$ as shown in Figs. 2(c-d). Note that the oscillations (inset of Fig. 2(a)) are achieved due to the balance between the energy supplied by STT and the energy dissipated by damping²². The switching time, that is the time for m_x to cross from -1 to +1, is plotted against current for different values of J_1 and J_2 in Fig. 2(e). The switching current, that is the current above which the switching takes place, can be obtained from Eq.(4). This equation implies that the switching current increases with J_1 and J_2 . Also, we can see that at a given value of current the switching time decreases with a decrease of J_1 or J_2 .

As we discussed before, oscillations are exhibited for the currents between I_c^{min} and I_c^{max} . To discuss the impact of the current on the frequency for different values of J_1 and J_2 , current versus frequency is plotted in Fig. 3(a) for $J_1 < 2J_2$. The oscillations of m_x is shown as inset of Fig.3(a) when $I = -3.5$ mA, $J_1 = 5$ mJ/m² and $J_2 = 4.5$ mJ/m². From Fig.3(a) we can understand that as the value of J_1 decreases the minimum current required to achieve the oscillations increases while when J_2 increases the maximum frequency attainable by the current also increases. Also, we can observe that the frequency can be increased by the current up to or above 300 GHz, which is the largest value achieved to date for the nanopillar shaped STNOs. To investigate the influence of J_1 on the frequency, Fig.3(b) is plotted for the frequency when $J_2 = 5$ mJ/m², where the nonoscillatory regions are represented by white color which includes two steady states (m_{x1}, m_{y1}, m_{z1}) for $J_1 < 2J_2$ and $(-1, 0, 0)$ for $J_1 \geq 2J_2$ below I_c^{min} , and one steady state $(1, 0, 0)$ above I_c^{max} . The critical currents I_c^{min} and I_c^{max} , which are obtained from Eqs.(5) and (4) respectively, are plotted as open circles and triangles in Fig. 3(b), respectively, match well with the numerical results. From Fig. 3(b) we can observe that there is a critical value for J_1 where $I_c^{max} = I_c^{min}$, namely J_1^c , below which there occur no oscillations due to the current. The value of J_1^c can be determined by equating the Eqs.(4) and (5) as

$$J_1^c = \frac{1}{3\lambda^2} \left(2J_2\lambda(3 + 2\lambda) - (Q + \sqrt{S})^{1/3} + \frac{J_2\lambda^3 R}{(Q + \sqrt{S})^{1/3}} \right), \quad (6)$$

where $P = (\lambda - 1)dM_s(H_k - 4\pi M_s)$, $Q = J_2^2\lambda^3(-9P\lambda(3 + \lambda) - 4J_2(-27 + \lambda(-27 + \lambda(27 + 43\lambda))))$, $R = 3P - 16J_2\lambda$ and $S = J_2^3\lambda^9 R^3 + Q^2$. As confirmed in Fig. 3(b), the value of J_1^c is 4.27 mJ/m² for $J_2 = 5$ mJ/m². For $J_1 < J_1^c$, the increase in current drives the magnetization to switch from (m_{x1}, m_{y1}, m_{z1}) to $(1, 0, 0)$ without any oscillations. For $J_1^c < J_1 < 2J_2$, the bilinear coupling decreases the value of I_c^{min} and increases the value of I_c^{max} , implying that the tunability range of the frequency increases. The output power of the STNO corresponding to $I = -4$ mA, d

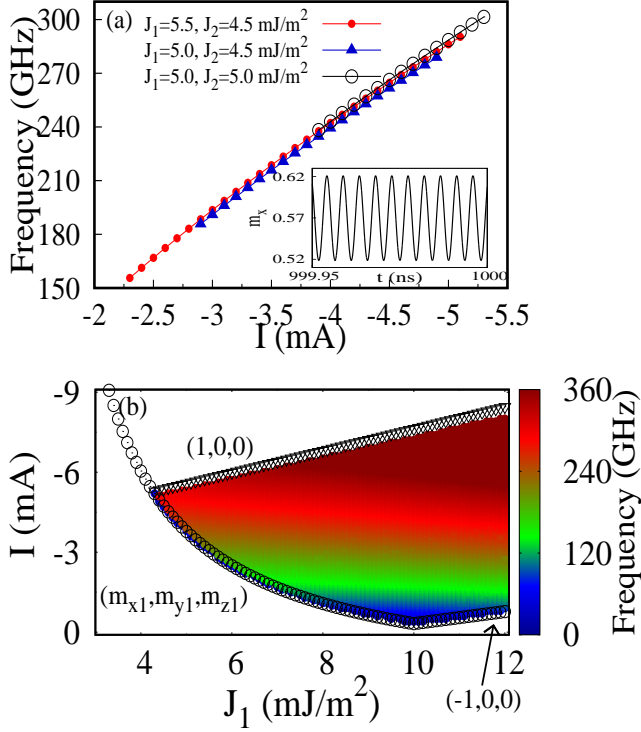


FIG. 3. (a) Variation of oscillations frequency for current. (Inset) Time evolution of m_x (216 GHz) for $I = -3.5$ mA and $J_1 = 5$ mJ/m², $J_2 = 4.5$ mJ/m². (b) Frequency variation due to the current and J_1 for $J_2 = 5$ mJ/m².

= 3.2 nm, $J_1 = 5$ mJ/m² and $J_2 = 4.5$ mJ/m² is determined as 0.41 nW. The impact of the current and the thickness of the free layer are investigated and found that they can enhance the power up to 20.91 and 1.69 times (see Appendix C).

IV. CONCLUSION

In conclusion, we have investigated the dynamics of a Co|RuFe|Co STNO with the bilinear and biquadratic couplings using the LLGS equation and identified that the magnetization may continue in the same state or switch from one state to another or oscillate depending upon the magnitude of the current. We have examined the current induced switching from anti-parallel to parallel alignment through steady oscillations. This field-free current induced switching may be helpful for low power consumption and efficient practical applications which are very robust against strong field disturbances²⁵. We have observed that within the oscillatory region the bilinear coupling can reduce the minimum current for the oscillations and increase the tunability range of the frequency. Similarly, the biquadratic coupling increases the maximum frequency that can be obtained by the current. We have shown that in the presence of bilinear and bi-

quadratic couplings the frequency can be enhanced above 300 GHz by the current. We believe that the experimental achievements on noncollinear alignments in STNO may provide greater avenue for applications related to microwave generation and current induced switching.

ACKNOWLEDGMENTS

The works of V.K.C. and R. G are supported by the DST-SERB-CRG Grant No. CRG/2020/004353 and they wish to thank DST, New Delhi for computational facilities under the DST-FIST programme (SR/FST/PS-1/2020/135) to the Department of Physics. M.L. wishes to thank the Department of Science and Technology for the award of a DST-SERB National Science Chair under Grant No. NSC/2020/00029 in which R. Arun is supported by a Research Associateship.

Appendix A: Identification of the orientation of \mathbf{m} in the absence of current by using microwave field

Before applying any current, the magnetization would settle in the xy -plane at $(m_{x0}, m_{y0}, m_{z0}) = (-1, 0, 0)$ when $J_1 \geq 2J_2$ or at $(-J_1/2J_2, \sqrt{1 - J_1^2/4J_2^2}, 0)$ when $J_1 < 2J_2$. The spherical polar coordinates corresponding to (m_{x0}, m_{y0}, m_{z0}) are given by $(\phi_0, \theta_0) = (\cos^{-1}(m_{x0}), \pi/2)$. In Fig.1(b) of the main text, the values of ϕ_0 for different values of J_1 and J_2 have been plotted (black downward triangles) from the time evolution of m_x as shown in Fig.1(a). The polar angle ϕ_0 where the magnetization would settle before applying any current can also be determined by applying a microwave field perpendicular (along z -axis) to the plane of the free layer. Let the effective field that includes the microwave field along positive z -direction be

$$\mathbf{H}_{eff} = ((H_k - 4\pi M_s)m_z + H_a \sin(2\pi ft)) \mathbf{e}_z - \frac{1}{dM_s}(J_1 + 2J_2 m_x) \mathbf{e}_x, \quad (\text{A1})$$

where the amplitude of the perpendicular microwave field $H_a = 100$ Oe and the frequency of the microwave field $f = 1$ GHz. When the microwave field is applied perpendicular to the plane, the magnetization \mathbf{m} will get perturbed about ϕ_0 from $\phi_0 - (\Delta\phi/2)$ to $\phi_0 + (\Delta\phi/2)$, where $\Delta\phi$ is the angular range of the perturbation. This perturbation of \mathbf{m} can be projected along any unit vector $\hat{\mathbf{m}}' (= \cos\psi \mathbf{e}_x + \sin\psi \mathbf{e}_y)$ along the direction ψ in the xy -plane. The component of the projected \mathbf{m} along \mathbf{m}' is given by $m_p = \mathbf{m} \cdot \mathbf{m}' = m_x \cos\psi + m_y \sin\psi$. The range of the projected \mathbf{m} along \mathbf{m}' can be determined as $\Delta m_p = m_p^{max} - m_p^{min}$, where the m_p^{max} and m_p^{min} are the maximum and minimum values of the projection m_p , respectively. Since the magnetization will get perturbed in the perpendicular direction to its initial orientation, the

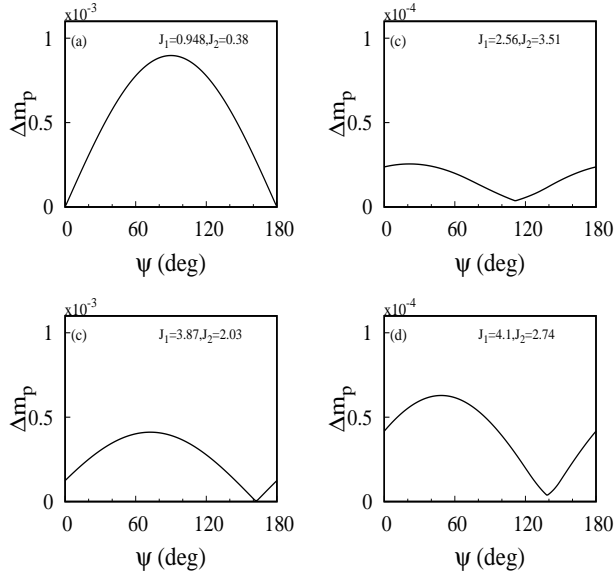


FIG. 4. Range of projected \mathbf{m} along different directions ψ . The plots have been plotted for different values of (J_1, J_2) (mJ/m^2).

value of Δm_p will be minimum when $\psi = \phi_0$ and maximum when $\psi = \phi_0 - 90^\circ$. The values of Δm_p against ψ for different pair of bilinear and biquadratic exchange coupling constants (J_1, J_2) mJ/m^2 are plotted in Fig. 4.

The minimum values of Δm_p indicates the angle of orientation of the magnetization ϕ_0 in the absence of current. From Fig. 4 we can identify the values of ϕ_0 corresponding to $(J_1 = 2.56, J_2 = 3.51)$ mJ/m^2 , $(4.1, 2.74)$ and $(3.87, 2.03)$ as 111° , 138° and 162° , respectively. The plot corresponding to $(0.948, 0.38)$ indicates two minimum values of ϕ_0 as 0° and 180° . Since the positive value of J_1 leads to antiferromagnetic coupling as we mentioned in the main text, ϕ_0 is 180° for $J_1 = 0.948$ mJ/m^2 and $J_2 = 0.38$ mJ/m^2 . These values of ϕ_0 exactly match with the experimental and numerical values of ϕ_0 plotted in Fig.1(b) of the main text.

Appendix B: Determination of critical currents

In this appendix, we briefly explain the procedure to determine the minimum and maximum critical currents between which the STNO exhibits the magnetization oscillations. Let us consider the LLGS equation (Eq.(1)) transformed into the spherical polar co-ordinates by using the transformation equations $m_x = \sin \theta \cos \phi$, $m_y =$

$\sin \theta \sin \phi$, $m_z = \cos \theta$:

$$\frac{d\theta}{dt} = \frac{\gamma}{1 + \alpha^2} \left\{ -P(\alpha \cos \theta \cos \phi - \sin \phi) - \alpha(H_k - 4\pi M_s) \sin \theta \cos \theta - H_{S0} \frac{(\alpha \sin \phi + \cos \theta \cos \phi)}{(1 + \lambda \sin \theta \cos \phi)} \right\} = M(\theta, \phi), \quad (\text{B1})$$

$$\frac{d\phi}{dt} = \frac{\gamma \csc \theta}{1 + \alpha^2} \left\{ P(\cos \theta \cos \phi + \alpha \sin \phi) + (H_k - 4\pi M_s) \sin \theta \cos \theta + H_{S0} \frac{(\sin \phi - \alpha \cos \theta \cos \phi)}{(1 + \lambda \sin \theta \cos \phi)} \right\} = N(\theta, \phi). \quad (\text{B2})$$

Here θ and ϕ are the polar and azimuthal angles, respectively, $H_{S0} = \hbar \eta I / 2e M_s V$ and $P = (J_1 + 2J_2 \sin \theta \cos \phi) / dM_s$. The nature of the stability of a fixed point (θ^*, ϕ^*) , where $M(\theta^*, \phi^*) = N(\theta^*, \phi^*) = 0$, can be identified from the eigen values of the Jacobian matrix,

$$J = \begin{pmatrix} \left. \frac{dM}{d\theta} \right|_{(\theta^*, \phi^*)} & \left. \frac{dM}{d\phi} \right|_{(\theta^*, \phi^*)} \\ \left. \frac{dN}{d\theta} \right|_{(\theta^*, \phi^*)} & \left. \frac{dN}{d\phi} \right|_{(\theta^*, \phi^*)} \end{pmatrix}, \quad (\text{B3})$$

associated with Eqs.(B1) and (B2) corresponding to (θ^*, ϕ^*) . The fixed point (θ^*, ϕ^*) will be stable only when the real parts of both the eigen values are negative. According to Routh-Hurwitz's criterion the real parts of both the eigen values will be negative if and only if the trace of the matrix J becomes negative,

$$\text{Tr}(J) < 0. \quad (\text{B4})$$

In the absence of the current $(\theta^*, \phi^*) = (\pi/2, \cos^{-1}(-J_1/2J_2))$ for $J_1 < 2J_2$ or $(\pi/2, \pi)$ for $J_1 \geq 2J_2$.

When $|I| < |I_c^{min}|$ and $J_1 < 2J_2$ the (θ^*, ϕ^*) is approximately equal to $(\pi/2, \cos^{-1}(-J_1/2J_2))$ and becomes stable where the magnetization settles. The trace of the matrix corresponding to $(\pi/2, \cos^{-1}(-J_1/2J_2))$ is given by

$$\text{Tr}(J)|_{(\theta^*, \phi^*)} = \frac{\gamma}{1 + \alpha^2} \left[\alpha(H_k - 4\pi M_s) - \frac{\alpha(4J_2^2 - J_1^2)}{2J_2 dM_s} + \frac{H_{S0}}{2J_2 - J_1 \lambda} \left(\frac{(4J_2^2 - J_1^2)^2}{2J_2 - J_1 \lambda} - 2H_{S0} J_1 \right) \right]. \quad (\text{B5})$$

The minimum critical current I_c^{min} (for $J_1 < 2J_2$), below which the fixed point $(\pi/2, \cos^{-1}(-J_1/2J_2))$ is stable, will be derived from the condition of stability (B4)

and by using the Eq.(B5) as

$$I_c^{min} = -\frac{eA\alpha(2J_2 - J_1\lambda)^2}{\hbar\eta J_2} \left[\frac{2J_2 dM_s(H_k - 4\pi M_s) - (4J_2^2 - J_1^2)}{\lambda(4J_2^2 - J_1^2) - 2J_2(2J_2 - J_1\lambda)} \right] \quad (B6)$$

Similarly, when $|I| < |I_c^{min}|$ and $J_1 \geq 2J_2$ the state $(\theta^*, \phi^*) = (\pi/2, \pi)$ becomes stable and the magnetization settles into $(-1, 0, 0)$. The trace of the matrix J corresponding to the $(\pi/2, \pi)$ is derived as

$$\text{Tr}(J)|_{(\pi/2, \pi)} = -\frac{\gamma}{(1 + \alpha^2)} \left[\frac{2H_{S0}}{1 - \lambda} - (H_k - 4\pi M_s)\alpha + \frac{2(J_1 - 2J_2)\alpha}{dM_s} \right]. \quad (B7)$$

From the condition (B4) and Eq.(B7), we can derive the minimum critical current (for $J_1 \geq 2J_2$) below which the $(\pi/2, \pi)$ is stable as

$$I_c^{min} = -\frac{eA\alpha(1 - \lambda)}{\hbar\eta} [2(J_1 - 2J_2) - dM_s(H_k - 4\pi M_s)]. \quad (B8)$$

When $|I| > |I_c^{max}|$ the magnetization state $(\theta^*, \phi^*) = (\pi/2, 0)$ becomes stable and the magnetization settles into $(1, 0, 0)$. The trace of the matrix J corresponding to $(\pi/2, 0)$ is

$$\text{Tr}(J)|_{(\pi/2, 0)} = \frac{\gamma}{1 + \alpha^2} \left[\frac{2(J_1 + 2J_2)\alpha}{dM_s} + \frac{2H_{S0}}{1 + \lambda} + (H_k - 4\pi M_s)\alpha \right]. \quad (B9)$$

The maximum critical current I_c^{max} , above which $(\pi/2, 0)$ becomes stable, can be derived from the condition (B4) and Eq.(B9) as

$$I_c^{max} = -\frac{\alpha eA(1 + \lambda)}{\hbar\eta} [2(J_1 + 2J_2) + (H_k - 4\pi M_s)dM_s]. \quad (B10)$$

Appendix C: Output power and its enhancement

The output power P corresponding to the output voltage V of an STNO is given by²⁶

$$P = \frac{V^2}{2R_L} = \frac{1}{2R_L} \left(\frac{I \Delta R R_L (\mathbf{m} \cdot \mathbf{p})}{2(R_{avg} + R_L)} \right)^2 = \frac{I^2 \Delta R^2 R_L m_x^2}{8(R_{avg} + R_L)^2}, \quad (C1)$$

where $\Delta R = R_{AP} - R_P$ and $R_{avg} = (R_{AP} + R_P)/2$. The quantities R_{AP} and R_P are the resistances while the STNO in antiparallel and parallel configuration, respectively. R_L is the load resistance across which the output

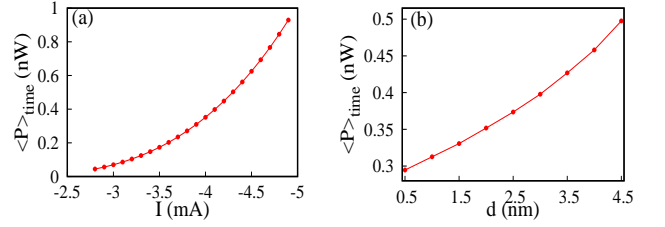


FIG. 5. The variation of time averaged power against (a) current for $d = 2$ nm and (b) thickness of the free layer for $I = -4$ mA. Here, $J_1 = 5$ mJ/m² and $J_2 = 4.5$ mJ/m².

power $\langle P \rangle_{time}$ is detected. The time averaged power is delivered as²⁶

$$\langle P \rangle_{time} = \frac{I^2 \Delta R^2 R_L}{8(R_{avg} + R_L)^2} \langle m_x^2 \rangle_{time}. \quad (C2)$$

The expression for R_{AP} can be calculated from the GMR ratio $\Delta R/R_P$ as $R_{AP} = R_P + (\Delta R/R_P)R_P$. Since the magnetoresistance for Co|RuFe|Co is not available in the literature, we consider the GMR ratio 0.004 corresponding to Co(3.2nm)|Ru(0.5nm)|Co(3.2nm) to find the approximated value of $\langle P \rangle_{time}$ for our system²⁷. For $R_P = 100 \Omega$, $R_L = 50 \Omega$ and $I = -4$ mA, $\langle P \rangle_{time}$ is determined from $\langle m_x^2 \rangle_{time}$ corresponding to the $m_x(t)$ between 950 ns and 1000 ns as 0.41 nW. The $\langle P \rangle_{time}$ is plotted for the different currents in Fig. 5(a) for $d = 2$ nm and different thicknesses of the free layer in Fig. 5(b) for $I = -4$ mA when $J_1 = 5$ mJ/m² and $J_2 = 4.5$ mJ/m². From Fig. 5(a) and (b) we can understand that the power can be enhanced by the current up to 20.91 times and the free layer's thickness up to 1.69 times corresponding to $J_1 = 5$ mJ/m² and $J_2 = 4.5$ mJ/m², which confirms the tunability and enhancement of power by the current and the thickness of the free layer. In general, the output power can be enhanced further by connecting the STNOs parallelly or serially and phase locking them by microwave field and current^{28,29}.

AUTHOR DECLARATIONS

Conflict of Interest

The authors have no conflicts to disclose.

DATA AVAILABILITY

The data that support the findings of this study are available from the corresponding author upon reasonable request.

¹J. C. Slonczewski, Phys. Rev. B **39** 6995 (1989); J. Magn. Mater. **159**, (1996); Phys. Rev. B **71**, 024411 (2005).

²L. Berger, Phys. Rev. B **54**, 9353 (1996).

- ³P. He, J. Gao, C. T. Marinis, P. V. Parimi, C. Vittoria and V. G. Harris, *Appl. Phys. Lett.* **93**, 193505 (2008).
- ⁴V. Sharma, Y. Khivintsev, I. Harward, B. K. Kuanr and Z. Celinski, *J. Magn. Magn. Mater.* **489**, 165412 (2019).
- ⁵B. Rana and Y. Otani *Commun. Phys.* **2**, 90 (2019).
- ⁶X. Han, X. Wang, C. Wan, G. Yu, and X. Lv, *Appl. Phys. Lett.* **118**, 120502 (2021).
- ⁷S. Fukami, C. Zhang, S. Dutttagupta, A. Kurenkov, and H. Ohno, *Nat. Mater.* **15**(5), 535-541 (2016).
- ⁸Y. Oh, S. C. Baek, Y. M. Kim, H. Y. Lee, K. Lee, C. Yang, E. Park, K. Lee, K. Kim, G. Go, J. Jeong, B. Min, H. Lee, K. Lee, and B. Park, *Nat. Nanotechnol.* **11**(10), 878–884 (2016).
- ⁹R. Arun, R. Gopal, V. K. Chandrasekar, and M. Lakshmanan, *J. Appl. Phys.* **127**, 153903 (2020).
- ¹⁰R. Arun, R. Gopal, V. K. Chandrasekar, and M. Lakshmanan, *IEEE Trans. Magn.* **56**, 1400310 (2020).
- ¹¹H. Kubota, K. Yakushiji, A. Fukushima, S. Tamaru, M. Konoto, T. Nozaki, S. Ishibashi, T. Saruya, S. Yuasa, T. Taniguchi, H. Arai, H. Imamura, *Appl. Phys. Express* **6**, 103003 (2013).
- ¹²L. Rehm, G. Wolf, B. Kardasz, M. Pinarbasi, A. D. Kent, *Appl. Phys. Lett.* **115**, 182404 (2019).
- ¹³F. Hooman, B. Tim, T. Mohammad, C. Jose Diogo, J. Alex, F. Ricardo, M. J.Kargaard, M.Farshad, *Front. Neurosci.* **13**, 1429 (2020).
- ¹⁴R. A. Duine, K. J. Lee, S. S. P. Parkin, M. D. Stiles, *Nat. Phys.* **14**, 217–219 (2018).
- ¹⁵P. Grunberg, R. Schreiber, Y. Pang, M. B. Brodsky, H. Sowers, *Phys. Rev. Lett.* **57**, 2442-2445 (1986).
- ¹⁶S. S. P. Parkin, *Phys. Rev. Lett.* **67**, 3598–3601 (1991).
- ¹⁷T. McKinnon and E. Girt, *App. Phys. Lett* **113**, 192407 (2018).
- ¹⁸P. Omelchenko, B. Heinrich, E. Girt, *Appl. Phys. Lett.* **113**, 142401 (2018).
- ¹⁹S. Peng, D. Zhu, J. Zhou, B. Zhang, A. Cao, M. Wang, W. Cai, K. Cao, and W. Zhao, *Adv. Electron. Matter.* **5**(8), 1900134 (2019).
- ²⁰X. Fan, G. Wei, X. Lin, X. Wang, Z. Si, X. Zhang, Q. Shao, S. Mangin, E. Fullerton, L. Jiang, W. Zhao, *Matter* **2**(6), 1582 (2020).
- ²¹Z. R. Nunn, C. Abert, D. Suess, E. Girt, *Sci. Adv.* **6**, eabd8861 (2020).
- ²²T. Taniguchi, S. Tsunegi, H. Kubota, H. Imamura, *Appl. Phys. Lett.* **104**, 152411 (2014).
- ²³J. Torrejon, M. Riou, F. A. Araujo, S. Tsunegi, G. Khalsa, D. Querlioz, P. Bortolotti, V. Cros, K. Yakushiji, A. Fukushima, H. Kubota, S. Yuasa, M. D. Stiles, and J. Grollier, *Nature* **547**, 428-431 (2017).
- ²⁴T. McKinnon, B. Heinrich, and E. Girt, *Phys. Rev. B* **104**, 024422 (2021).
- ²⁵L. Liu, Q. Qin, W. Lin, C. Li, Q. Xie, S. He, X. Shu, C. Zhou, Z. Lim, J. Yu, W. Lu, M. Li, X. Yan, S. J. Pennycook, J. Chen, *Nat. Nanotechnol.* **14**, 939 (2019).
- ²⁶S. E. Russek, W. H. Rippard, T. Cecil and R. Heindl, Chapter 38, *Handbook of Nanophysics: Functional Nanomaterial [M]*, CRC PrLLic, 2010.
- ²⁷K. Rahmouni, A. Dinia, D. Stoeffler, K. Ounadjela, *Phys. Rev. B* **59**, 9475 (1999).
- ²⁸S. Kaka, M. R. Pufall, W. H. Rippard, T. J. Silva, S. E. Russek, J. A. Katine, *Nature* **437**, 389 (2005).
- ²⁹R. Lebrun, S. Tsunegi, P. Bortolotti, H. Kubota, A.S. Jenkins, M. Romera, K. Yakushiji, A. Fukushima, J. Grollier, S. Yuasa, V. Cros, *Nat. Commun.* **8**, 15825 (2017).